Pax3:Fkhr interferes with embryonic *Pax3* and *Pax7* function: implications for alveolar rhabdomyosarcoma cell of origin

Charles Keller,[1] Mark S. Hansen,[1] Cheryl M. Coffin,[2] and Mario R. Capecchi[3,4]

[1]Division of Pediatric Hematology-Oncology, Department of Pediatrics, [2]Division of Pediatric Pathology, Department of Pathology, and [3]Howard Hughes Medical Institute and Department of Human Genetics, University of Utah, Salt Lake City, Utah 84112, USA

To investigate the role of the translocation-associated gene *Pax3:Fkhr* in alveolar rhabdomyosarcomas, we generated a Cre-mediated conditional knock-in of *Pax3:Fkhr* into the mouse *Pax3* locus. Exploring embryonic tumor cell origins, we replaced a *Pax3* allele with *Pax3:Fkhr* throughout its expression domain, causing dominant-negative effects on *Pax3* and paradoxical activation of the Pax3 target gene, c-*Met*. Ectopic neuroprogenitor cell proliferation also occurs. In contrast, activation later in embryogenesis in cells that express *Pax7* results in viable animals with a postnatal growth defect and a moderately decreased Pax7+ muscle satellite cell pool, phenocopying *Pax7* deficiency but remarkably not leading to tumors.

Supplemental material is available at http://www.genesdev.org.

Received July 26, 2004; revised version accepted September 3, 2004.

A t(2;13) translocation forms the *Pax3:Fkhr* fusion gene in 55%–75% of cases for the childhood muscle cancer, alveolar rhabdomyosarcoma (Sorensen et al. 2002). This novel chimeric gene encodes for a transcription factor possessing the paired box and homeodomain DNA-binding domains from the transcription factor *Pax3* fused to the potent transactivation domain of the *Fkhr* transcription factor (Sorensen et al. 2002). *Pax3:Fkhr* is believed to result in a molecular gain of function that may initiate a deregulated muscle development program in the affected cells.

The roles of *Pax3* and *Pax7* are best defined in embryogenesis, where they are important transcription regulatory factors in neural tube and myogenic development (Jostes et al. 1990; Goulding et al. 1991). Studies of *Pax3*-defective *Splotch* (Auerbach 1954) mice have revealed that *Pax3* is an important determinant of p53-dependent dorsal neural tube closure (Pani et al. 2002) and an essential factor for proliferation and migration of muscle precursors from the presomitic mesoderm (Tremblay et al. 1998). *Pax7* is most closely related to *Pax3*, and in general parallels the expression pattern of *Pax3* with a slight delay in expression onset (Jostes et al. 1990). Whereas *Pax3*-defective mice fail to form embryonic hypaxial and epaxial muscles (Tremblay et al. 1998), *Pax7*-deficient mice have grossly normal embryonic muscle mass but are impaired in the ability form muscle stem cell (satellite cell)-derived postnatal muscle (Oustanina et al. 2004), which normally accounts for a substantial proportion of adult muscle mass.

In an accompanying paper (Keller et al. 2004), we demonstrate that activation of *Pax3:Fkhr* in a target pool of Myf6+ differentiating muscle produces alveolar rhabdomyosarcoma. In this paper, we determine molecular actions of Pax3:Fkhr by studying its perturbation of well-characterized processes: normal mouse embryogenesis, embryonic myogenesis, and postnatal satellite cell-derived myogenesis. The in vivo functions of Pax3:Fkhr during embryogenesis also provide important insight into the potential timing and cell(s) of origin for this tumor. Most importantly, we demonstrate the surprising result that *Pax3:Fkhr* expression in Pax7+ satellite cells does not lead to rhabdomyosarcomas.

Results and Discussion

The conditional *Pax3:Fkhr* (P3Fm) knock-in allele, which allows normal *Pax3* expression of that allele until Cre is present, is described in the accompanying paper (Keller et al. 2004) and Supplementary Figure S1A. The complementary *Pax7*-driven *Cre* allele was designed to allow *Cre* expression in the *Pax7* expression domain without interfering with the normal Pax7 function (see Materials and Methods; Supplementary Fig. S1B). $Pax7^{ICNm/wt}$ and $Pax7^{ICNm/ICNm}$ mice are phenotypically normal and fertile. To determine whether this Cre was expressed in the expected *Pax7* expression domain, lineage analysis was performed by crossing $Pax7^{ICNm/wt}$ mice to *ROSA26* LacZ reporter mice (Sorriano 1999). Doubly heterozygous $Pax7^{ICNm/wt}$ $Gtrosa26^{tm1Sor/wt}$ embryos were harvested at embryonic days 10 and 12 (E10 and E12) (Supplementary Fig. S1C,D, respectively). LacZ expression recapitulates the previously described pattern of *Pax7* expression (Mansouri et al. 1996) in the somites, midface, and neural tube-derived structures.

Pediatric cancers are frequently associated with chromosomal translocations, and these translocations are often asymptomatically present at birth (Greaves and Wiemels 2003). To replicate a prenatal *Pax3:Fkhr* translocation for alveolar rhabdomyosarcomas, we triggered *Pax3:Fkhr* in the *Pax3* expression domain from the earliest time point of *Pax3* promoter activation by breeding conditional $Pax3^{P3Fm/wt}$ mice to transgenic mice expressing *Cre* ubiquitously from early gestation (Schwenk et al. 1995) (we denote this transgene locus as *RajCreTg*). The *Pax3:Fkhr* transcript was confirmed by sequencing the RT–PCR product of $Pax3^{P3Fa/wt}$ $RajCreTg^{Cre/wt}$ E10.5 embryos (see Supplementary Fig. S2). $Pax3^{P3Fa/wt}$ $RajCreTg^{Cre/wt}$ mice were born in normal Mendelian ratios but displayed severe birth defects (see Fig. 1A–D and its legend). Elements of this phenotype are reminiscent of the *Splotch* (Auerbach 1954) and *Splotch-delayed*

[*Keywords*: Alveolar rhabdomyosarcoma; *Pax3:Fkhr*; *Pax7*; *FoxO1A*; chromosomal translocation; satellite cell]
[4]Corresponding author.
E-MAIL mario.capecchi@genetics.utah.edu; FAX (801) 585-3425.
Article and publication are at http://www.genesdev.org/cgi/doi/10.1101/gad.1243904.

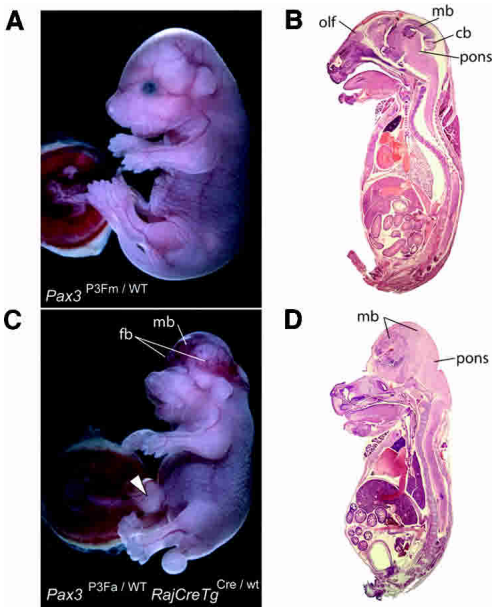

Figure 1. Early embryonic activation of *Pax3:Fkhr*. (*A*,*B*) Whole-mount and sagittal section of an unaffected E18.5 embryo harboring a single *Pax3:Fkhr* allele ($Pax3^{P3Fm/wt}$) that had not been activated by Cre. (*C*,*D*) Whole-mount and sagittal section of a mutant E18.5 embryo harboring a single *Pax3:Fkhr* allele that has been activated by the Rajewsky Cre driver ($Pax3^{P3Fa/wt}$ $RajCreTg^{Cre/wt}$). Note cranioschisis, exencephaly, anophthalmia, omphalocoele (open arrowhead), foreshortened snout, and slightly foreshortened limbs. In the mutant, the forebrain (fb) is hypoplastic and laterally displaced by the midbrain. Note absence of the cerebellum (cb) and olfactory lobe (olf), as well as overproliferation and anteriorization of the midbrain (mb).

(Tremblay et al. 1998) homozygous mutant phenotypes. This partial phenocopy of *Pax3* deficiency includes cranioschisis, exencephaly, and midface abnormalities (Tremblay et al. 1998) and characteristic skeletal dysplasia (see Supplemental Material; Supplementary Fig. S3). The hypoplastic dorsal root ganglia, normally organized but hypoplastic limb muscle, and thinned diaphragm of $Pax3^{P3Fa/wt}$ $RajCreTg^{Cre/wt}$ mice are similar but do not fully phenocopy the absent dorsal root ganglia, absent hypaxial (limb) muscle, and absent diaphragm reported for *Splotch* mice (see Supplementary Fig. S4). $Pax3^{P3Fa/wt}$ $RajCreTg^{Cre/wt}$ mice had normal respiratory competency for several hours under isothermal conditions. Phenotypes of *Splotch* mice not present in $Pax3^{P3Fa/wt}$ $RajCreTg^{Cre/wt}$ mice include spina bifida of incomplete penetrance and cardiac conotruncal defects (truncus arteriosus, ventricular septal defects), whereas $Pax3^{P3Fa/wt}$ $RajCreTg^{Cre/wt}$ mice have distinctive phenotypes such as forebrain hypoplasia, anophthalmia, disorganized midbrain overgrowth, and omphalocoele.

We concluded that $Pax3^{P3Fa/wt}$ $RajCreTg^{Cre/wt}$ mice partially phenocopy the *Splotch* and *Splotch-delayed* phenotypes for *Pax3* deficiency, suggesting the activity of the single wild-type allele of *Pax3* in $Pax3^{P3Fa/wt}$ $RajCreTg^{Cre/wt}$ mice is at least partially suppressed by the dominant-negative action of *Pax3:Fkhr*; however, novel features of our mice suggested that *Pax3:Fkhr* has additional embryonic targets as well.

We explored the midbrain overgrowth of newborn $Pax3^{P3Fa/wt}$ $RajCreTg^{Cre/wt}$ mice to determine whether these cells had undergone hamartomatous or neoplastic transformation. By histology (Fig. 2A,B), the midbrain and cortex was highly disorganized. Pseudorosettes with a high mitotic index were present in an increasing caudal-to-rostral gradient within the midbrain (Fig. 2C–F). Immunohistochemistry to determine the lineage of the pseudorosetting cells revealed that they express neuron-specific enolase (Fig. 2E) but not the markers of mature neuronal (synaptophysin, PGP9.5, S100, 68-kDa neurofilament, β-3-tubulin), glial (GFAP), ependymal (AE1.3), or mesenchymal (myogenin, desmin, vimentin) differentiation (data not shown). Electron microscopy revealed cells with high nuclear-to-cytoplasmic ratios without neurofilaments or other distinguishing features (data not shown). Because of the apparent undifferentiated state of these cells, we tested them for the expression of Sox1 (Fig. 2F), a marker of primitive embryonic neural stem cells (Aubert et al. 2003), which was positive. We therefore suggest that these ectopic, mitotically active cells represent retained primitive neuroectodermal precursors. The mitogenic effect *Pax3:Fkhr* has on Sox-1-expressing neural stem cells in the midbrain is especially interesting from the point of view that there may be tissue-specific cofactors that allow Pax3:Fkhr to induce proliferation in these cells but not others. This result also raises the interesting possibility that mechanisms underlying this *Pax3:Fkhr*-mediated neural stem cell proliferation could be elucidated and used for expansion of primitive embryonic neural stem cells in other contexts.

It is especially interesting that Pax3:Fkhr appears to

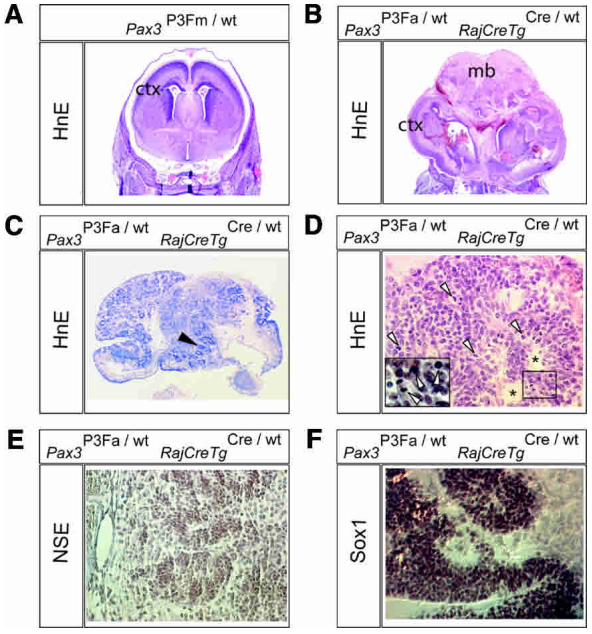

Figure 2. Overproliferation of primitive neuroectodermal cells for early embryonic activation of *Pax3:Fkhr*. Histological (HnE) brain sections of a $Pax3^{P3Fm/wt}$ E18.5 embryo (*A*) and a mutant $Pax3^{P3Fa/wt}$ $RajCreTg^{Cre/wt}$ E18.5 embryo (*B–F*). (*A*,*B*) Coronal section showing a global disorganization of the cortex (ctx) and overgrowth of the midbrain (mb) for mutant embryos. (*C*) More anterior coronal section of the mutant showing multiple zones of proliferation characterized by pseudorosettes (black arrowheads). (*D*) High-power view of pseudorosettes (asterisks) demonstrating multiple mitotic figures (open arrowheads and *inset*). (*E*) Positive immunohistochemical staining of pseudorosetting cells for neuron-specific enolase (NSE). (*F*) Positive Sox1 immunohistochemical staining of pseudorosetting cells from the anterior-most region of the mutant midbrain.

have these previously unsuspected gain-of-function properties in tissues of the optic placode and midbrain whose patterning and development are known to be affected by other Pax family members. Although Pax2 and Pax6 expression was preserved (see Supplemental Material; Supplementary Fig. S6), it remains possible that Pax3:Fkhr alters expression of downstream *Eya*, *Six*, *Dach*, and *Groucho* genes that normally interact with these *Pax* genes during development. It will be useful to take into account the recent report of transfection experiments (Xia and Barr 2004) for which oncogenic or growth suppressive effects of *Pax3:Fkhr* were correlated with low versus high expression levels, respectively.

Because of the similarity of our $Pax3^{P3Fa/wt}$ $RajCreTg^{Cre/wt}$ phenotype to the *Splotch* phenotype of homozygous *Pax3* deficiency, we tested whether *Pax3:Fkhr* was expressed in the expected *Pax3* domain or ectopically in a pattern influenced by 3′ *Fkhr* genomic regulatory elements, and whether expression of the normal allele of *Pax3* was affected. The eYFP marker for *Pax3:Fkhr* was expressed strongly in a pattern consistent with normal *Pax3* promoter activity (see Fig. 3A,B and its legend). RNA in situ hybridization using a riboprobe specific for the wild-type allele of *Pax3* revealed complete absence of wild-type *Pax3* expression (Fig. 3C) in the $Pax3^{P3Fa/wt}$ $RajCreTg^{Cre/wt}$ E10.5 mutant embryo, establishing that *Pax3:Fkhr* suppresses *Pax3* transcript levels. Immunohistochemistry using an antibody specific to the C terminus of wild-type Pax3 protein confirmed the near-complete absence of Pax3 in the $Pax3^{P3Fa/wt}$ $RajCreTg^{Cre/wt}$ mutant (Fig. 3D). This absence of *Pax3* transcripts and protein accounts for the similarities to the *Splotch* phenotype.

The mechanism for the decreased *Pax3* transcript level remains to be determined; however, in *Pax3:Fkhr*-expressing human tumor cell lines, the level of *Pax3* mRNA is fivefold lower than the level of *Pax3:Fkhr* mRNA (Davis and Barr 1997) despite similar RNA stabilities, suggesting a transcriptional level of action. Because *Pax3* transcription is positively autoregulated by its own protein product (Ridgeway and Skerjanc 2001), a reasonable model for suppression of *Pax3* transcription by Pax3:Fkhr is that the fusion protein negatively regulates *Pax3* transcription through the *Pax3 cis*-autoregulatory element.

To account for the differences between the $Pax3^{P3Fa/wt}$ $RajCreTg^{Cre/wt}$ phenotype and *Splotch*, we examined expression of the *Pax3*-related gene, *Pax7*, and downstream targets of Pax3. For *Pax7* expression, we generated mutant and normal E11.5 embryos carrying a targeted replacement of *Pax7* with *LacZ* (Mansouri et al. 1996). Pax7–LacZ expression was present in the $^{P3Fa/wt}RajCreTg^{Cre/wt}$ mutant, but Pax3–Pax7-derived structures such as the neural tube, dorsal root ganglia, and dermomyotome were perturbed (Fig. 3E,F). To determine whether Pax3:Fkhr may partially compensate for Pax3 loss in hypaxial muscle, we examined expression of a Pax3 downstream target gene, c-Met, in cells of the dermomyotome that migrate into the forelimb at E10.5 (Fig. 3G,H). Despite the absence of Pax3 in the $Pax3^{P3Fa/wt}$ $RajCreTg^{Cre/wt}$ mutant embryo, c-Met expression was increased and found to be coexpressed with the *Pax3:Fkhr* marker, eYFP. This result demonstrates that Pax3:Fkhr may partially compensate for Pax3 loss by transcriptional activation of some Pax3 target genes in developing hypaxial muscle. This result is also consistent with in vitro data demonstrating that c-Met is a target of Pax3:Fkhr (Ginsberg et al. 1998). Interestingly, broad activation of the c-Met signaling pathway in conjunction with inactivation of the *Ink4a/ARF* locus results in non-alveolar rhabdomyosarcomas in mice at high frequency (Sharp et al. 2002).

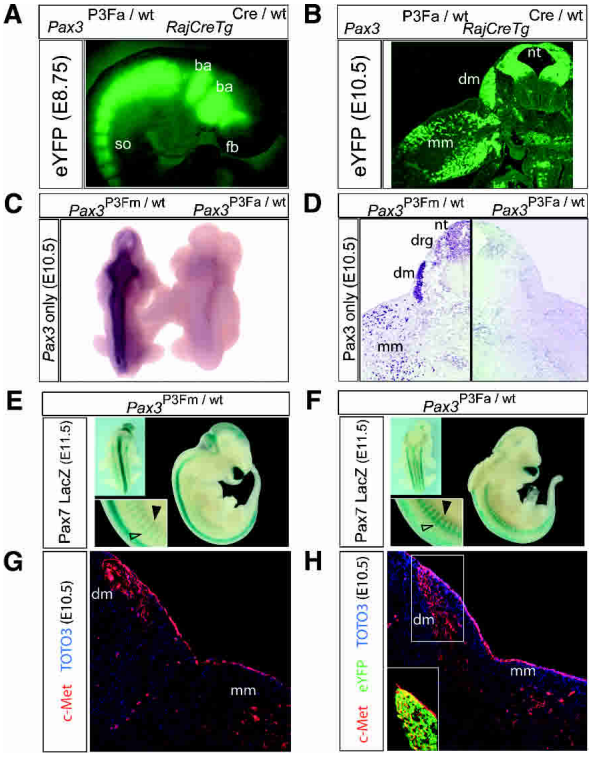

Figure 3. *Pax3:Fkhr*, *Pax3/7*, and target gene expression with early embryonic activation of *Pax3:Fkhr*. (*A*) Expression of the *Pax3:Fkhr* marker, eYFP, in somites (so), branchial arches (ba), and anterior forebrain (fb) of an E8.75 embryo. (*B*) eYFP marker of *Pax3:Fkhr* expression in a transverse section of the forelimb of an E10.5 $Pax3^{P3Fa/wt}$ $RajCreTg^{Cre/wt}$ embryo. (nt) Neural tube; (dm) dermomyotome; (mm) migrating myoblasts. (*C*) Whole-mount RNA in situ hybridization using a probe specific for only wild-type *Pax3*. (*Right*) Neural tube signal is absent for the mutant $Pax3^{P3Fa/wt}$ $RajCreTg^{Cre/wt}$ embryo. (*D*) Immunohistochemistry demonstrates near complete absence of wild-type Pax3 protein in the mutant $Pax3^{P3Fa/wt}$ $RajCreTg^{Cre/wt}$ embryo in an axial section of the forelimb. (*E*,*F*) Expression of Pax7 using a LacZ reporter reveals preserved Pax7 expression in the unaffected $Pax3^{P3Fm/wt}$ (*E*) and the mutant $Pax3^{P3Fa/wt}$ $RajCreTg^{Cre/wt}$ (*F*) embryo. However, the neural tube (*F*, *upper left inset*), dorsal root ganglia, and dermomyotome (*F*, *lower left inset*, open and black arrowheads, respectively) were severely perturbed. (*G*) Immunohistochemistry for c-Met in an axial cross-section of the unaffected $Pax3^{P3Fm/wt}$ embryo at the level of the forelimb. (*H*) c-Met immunohistochemistry in an axial section of the mutant $Pax3^{P3Fa/wt}$ $RajCreTg^{Cre/wt}$ embryo, demonstrating maintenance of c-Met expression despite Pax3 absence. (*Inset*) The eYFP marker of Pax3:Fkhr expression is coexpressed in c-Met-expressing cells of the dermomyotome (yellow).

To study the consequences of later embryonic activation of *Pax3:Fkhr* in the overlap of *Pax3* and *Pax7* expression domains, we bred conditional *Pax3:Fkhr* mice to *Pax7–Cre* mice. $Pax3^{P3Fa/wt}$ $Pax7^{ICNm/wt}$ pups were represented at normal Mendelian ratios and displayed the mild birth defects of a narrowed nose (Fig. 4A). Although initially equal in size to $Pax3^{P3Fm/wt}$ $Pax7^{wt/wt}$ littermates, the $Pax3^{P3Fa/wt}$ $Pax7^{ICNm/wt}$ pups showed evidence of severe postnatal growth retardation by age 3

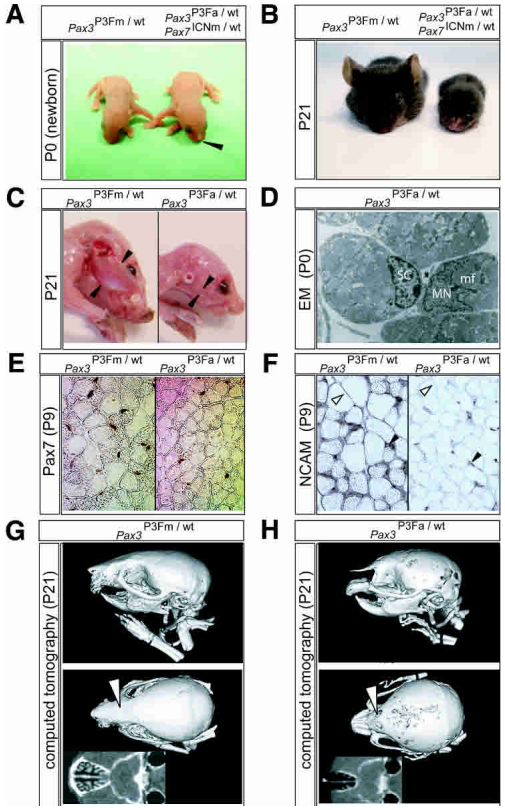

Figure 4. Phenotype caused by later embryonic activation of *Pax3:Fkhr* in the *Pax7* expression domain. (*A*) P0 mouse pups harboring a single *Pax3:Fkhr* allele not activated by Cre ($Pax3^{P3Fm/wt}$ $Pax7^{wt/wt}$, *left*) or a single *Pax3:Fkhr* allele that had been activated by *Pax7–Cre* ($Pax3^{P3Fa/wt}$ $Pax7^{ICNm/wt}$, *right*). Note pointed nose of the mutant (black arrowhead). (*B*) Severe runting at P21 of the mutant (*right*, weight 3 g) compared with the unaffected pup (*left*, 10.5 g). (*C*) Reduced masseter muscle mass (flanked by black arrowheads) of the pointed-nose mutant (*right*) in comparison to the unaffected control (*left*). (*D*) Electron microscopy (12,838×) demonstrating the presence of satellite cells, SC, in $Pax3^{P3Fa/wt}$ $Pax7^{ICNm/wt}$ mice. (MN) Myofiber nucleus; (mf) adjacent myofibrils. (*E*) Pax7 immunohistochemistry demonstrating lower satellite cell frequency and one-third smaller myofiber cross-sectional diameter in vastus lateralis skeletal muscle of $Pax3^{P3Fa/wt}$ $Pax7^{ICNm/wt}$ mutant mice (*right*) compared with $Pax3^{P3Fm/wt}$ $Pax7^{wt/wt}$ control mice (*left*). (*F*) Immunohistochemistry for NCAM, demonstrating cell surface expression in myofibers of $Pax3^{P3Fm/wt}$ $Pax7^{wt/wt}$ control mice (*left*) but not mutant $Pax3^{P3Fa/wt}$ $Pax7^{ICNm/wt}$ mice (*right*). NCAM expression is present in satellite cells (black arrowheads) from both animals. (*G*,*H*) Computed tomography 46-μm^3 resolution scans of the unaffected (*G*) and mutant (*H*) P21 pup skulls. Note absence of the rostral portion of the premaxilla (pm), hypoplasia of the lacrimal bones (open arrows), and hypoplasia of the nasal turbinates (*insets*).

wk, at which time they weighed less than one-third of their unaffected littermates (Fig. 4B). The reduced weight of the postnatal day 21 (P21) neonates is primarily the result of extreme reduction of muscle mass (Fig. 4C), with an accompanying mild reduction in myofiber diameter by histology (data not shown). To determine whether this reduction in muscle mass was a consequence of reduced satellite cells (Oustanina et al. 2004), electron microscopy was performed, revealing that satellite cells were present in normal weight $Pax3^{P3Fa/wt}$ $Pax7^{ICNm/wt}$ mutant P0 pups (Fig. 4D), but in fewer numbers than control littermates. To determine more precisely whether the number of satellite cells was reduced in $Pax3^{P3Fa/wt}$ $Pax7^{ICNm/wt}$ mice postnatally, we harvested the vastus lateralis muscle of P9 mouse pups and performed Pax7 immunohistochemistry to detect satellite cells, counterstaining myofiber nuclei with DAPI (Fig. 4E). We found a significant reduction in the percentage of satellite cells for mutant muscle compared with normal (10% vs. 15.2%, $p < 0.001$, $n = 11{,}805$ nonvessel nuclei counted). Myofiber density was significantly higher in mutants as compared with normals (515 vs. 349 cells per field, $p < 0.001$) as a result of reduced cross-sectional area of individual myofibers (affected myofiber cross-sectional area was 68% of control), which is similar to findings for $Pax7^{-/-}$ mice (Oustanina et al. 2004). The proportion of activated myoblasts coexpressing Pax7 and Myogenin in mutant and control mice appear comparable (data not shown); however, immunohistochemical staining for NCAM, a cell surface marker of myofibers that have undergone fusion with a satellite-cell-derived myoblast (Covault et al. 1986), showed severely reduced NCAM expression at the surface of mature myofibers from $Pax3^{P3Fa/wt}$ $Pax7^{ICNm/wt}$ mutant mice (Fig. 4F). Taken together, these results suggest that the small myofiber diameter at P21 is a result of the smaller satellite cell pool that is impaired in self-renewal capacity as are $Pax7^{-/-}$ mice (Oustanina et al. 2004), resulting in fewer satellite-cell-derived activated myoblasts being available to fuse with existing mature myofibers. This functional defect appears to have been present at birth but was significantly exacerbated postnatally.

For the midface defects, computed tomography scan at P21 demonstrated maxillary and lacrimal bone hypoplasia, agenesis of the rostral premaxilla, and severely underdeveloped nasal turbinates relative to control littermates (Fig. 4G,H). Because of the increased work of breathing associated with a collapsible nasal airway, only a limited number of $Pax3^{P3Fa/wt}$ $Pax7^{ICNm/wt}$ mice have survived to 3.5 mo of age (lethality was in part ameliorated by serial fostering followed by weaning to a gel-based source of hydration). None of these animals having ubiquitous *Pax3:Fkhr* rearrangements in their Pax7+ satellite cells developed alveolar rhabdomyosarcoma; this is a remarkable observation, because it is widely thought that alveolar rhabdomyosarcomas arise from satellite cells.

Collectively, the reduced muscle mass, maxillary and lacrimal bone hypoplasia, and nasal turbinate abnormalities of $Pax3^{P3Fa/wt}$ $Pax7^{ICNm/wt}$ mice strongly suggest a phenocopy of the *Pax7* deficiency (Mansouri et al. 1996; Oustanina et al. 2004). To determine whether the *Pax3:Fkhr* allele was directly suppressing *Pax7* transcription, we bred a *ROSA26* LacZ reporter gene (Sorriano 1999) into $Pax3^{P3Fa/wt}$ $Pax7^{ICNm/wt}$ mutant mice and controls to act as a readout of *Pax7* promoter activity and cell survival in E10.5 and E11.5 embryos (Fig. 5A–D). We encountered a range of LacZ reporter activity for which the *Pax7* promoter activity of $Pax3^{P3Fa/wt}$ $Pax7^{ICNm/wt}$ mice was either equivalent or increased as compared with $Pax3^{wt/wt}$ $Pax7^{ICNm/wt}$ control mice. An example of increased activity is shown in Figure 5A–D. The increased expression of *Pax7* in $Pax3^{P3Fa/wt}$ $Pax7^{ICNm/wt}$ mice may be understood in terms of *Pax3:Fkhr*-mediated suppression of *Pax3* expression, because Pax3 is normally a repressor of *Pax7* expression (Borycki et al. 1999) (in other words, Pax7 expression increases because Pax3 no longer suppresses *Pax7* transcription). At the protein level, Pax7 was also found to be increased in the neural

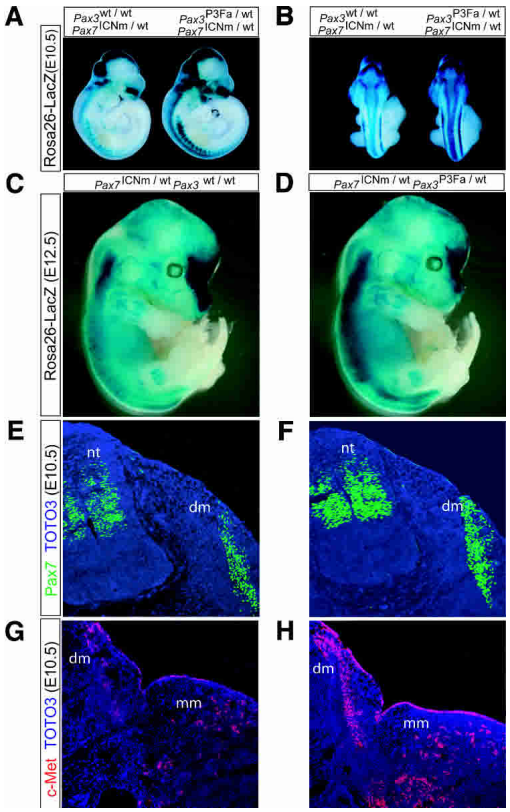

Figure 5. *Pax7* and c-Met expression with embryonic activation of *Pax3:Fkhr* in the *Pax7* expression domain. (*A*,*B*) *Rosa26* LacZ reporter activity in E10.5 embryos harboring a targeted *Pax7–Cre* allele alone ($Pax7^{ICNm/wt}$, *left*) or a targeted *Pax7–Cre* allele and a single, activated *Pax3:Fkhr* allele ($Pax3^{P3Fa/wt}$ $Pax7^{ICNm/wt}$, *right*). Reporter activity suggests maintenance or increased level of *Pax7* promoter activity in the neural tube and somites, as well as new *Pax7* promoter activity in the maxillary and mandibular branches of branchial arch 1. (*C*,*D*) Unaffected (*C*) and affected (*D*) E12.5 embryos demonstrating sustained *Pax7* promoter activity. (*E*,*F*) Pax7 immunohistochemistry in an axial cross-section at the level of the forelimb of the unaffected and affected embryos, demonstrating maintenance of Pax7 protein expression. (*G*,*H*) c-Met immunohistochemistry in an axial cross-section at the level of the forelimb of the unaffected and affected embryos, demonstrating increased expression of c-Met in the affected embryo (*H*).

tube and dermomyotome of $Pax3^{P3Fa/wt}$ $Pax7^{ICNm/wt}$ E10.5 embryos (Fig. 5E,F). As before for severely affected $Pax3^{P3Fa/wt}$ $RajCreTg^{Cre/wt}$ mutant embryos, the structurally less perturbed $Pax3^{P3Fa/wt}$ $Pax7^{ICNm/wt}$ E10.5 embryos demonstrated increased expression of the Pax3 downstream target, c-Met (Fig. 5G,H). This *Pax7* knockout phenocopy, despite increased Pax7 expression, could be explained by dominant-negative effects of Pax3:Fkhr on Pax7 targets, rather than effects on expression of *Pax7* itself. Unfortunately, at present downstream targets unique to Pax7 but not shared by Pax3 remain to be identified. A working model for how Pax3:Fkhr modulates Pax3, Pax7, and other downstream targets is shown in Supplementary Figure S7.

Recent transfection studies have shown that in embryonal rhabdomyosarcoma cells forced to express the alveolar rhabdomyosarcoma oncogene Pax3:Fkhr, Pax3 levels are increased and Pax7 levels are decreased (Tomescu et al. 2004). We have no clear explanation for the differences between this study and ours, except to suggest that embryonal rhabdomyosarcomas may not be the starting point or an equivalent cellular context for alveolar rhabdomyosarcomas.

In important previous studies, germ-line expression of the *Pax3:Fkhr* fusion gene under the control of the *Pax3* promoter has resulted in embryonic lethality without midbrain overproliferation, anophthalmia, or forebrain abnormalities (for references and comparisons, see Supplementary Table 1). In several instances, the other models represent hypomorphs of the early embryonic activation of our conditional model. However, each of these *Pax3:Fkhr* alleles had design differences such as being a transgene or being constructed from an incomplete cDNA instead of genomic DNA that may have affected the spectrum of *Pax3:Fkhr* activities in separate tissues. In our conditional knock-in model, we closely recapitulate the *cis*-regulatory changes caused by the real translocation in human tumors. At the time of Cre expression, we remove the 3 kb of *Pax3* containing exons 8–10 and juxtapose a previously silent 9.3-kb genomic fragment of *Fkhr* containing exons 2 and 3 and the full 3′-untranslated region. By using murine genomic DNA from both *Pax3* and *Fkhr*, we avoided potential complications of species-specific regulatory element sequence. The value of this approach is demonstrated by the markedly different phenotypes we see in our mice with early embryonic activation of *Pax3:Fkhr*. Furthermore, with this conditional model we have the added advantage of studying the effects of *Pax3:Fkhr* at midgestation, thereby bypassing the earlier *Pax3:Fkhr* expression that we show results in massive perturbation of the central nervous system. The later, less severe (yet intriguing) phenocopy of *Pax7* deficiency we report here allows for closer comparisons of gene expression levels in tissues whose structures are not so severely perturbed.

With regard to the timing and cell of origin for human tumors possessing *Pax3:Fkhr* translocations, the severity of birth defects in $Pax3^{P3Fa/wt}$ $RajCreTg^{Cre/wt}$ or $Pax3^{P3Fa/wt}$ $Pax7^{ICNm/wt}$ mice and associated lethality suggests that the translocation event in humans is unlikely to occur either as a germ-line mutation or as a mosaic in a broad range of embryonic myogenic precursors. One could speculate that a small subset of embryonically or postnatally derived Pax3/Pax7-coexpressing satellite cells could give rise to an alveolar rhabdomyosarcoma; however, our results demonstrate that $Pax3^{P3Fa/wt}$ $Pax7^{ICNm/wt}$ mice carrying the activated *Pax3:Fkhr* allele in the entire Pax7+ subcompartment of the satellite cell pool do not develop tumors even up to 3.5 mo of age, well into the young adulthood of these mice. This unexpected result that Pax7+ satellite cells do not give rise to alveolar rhabdomyosarcomas is made more remarkable by the observation in the accompanying paper (Keller et al. 2004) that *Pax3:Fkhr* activation in a target pool of Myf6+ differentiating myofibers leads to alveolar rhabdomyosarcoma tumors. These provocative findings, that mature differentiating skeletal muscle and not satellite cells gives rise to alveolar rhabdomyosarcomas, asks us to reconsider the widely held assumption that only muscle stem cells give rise to rhabdomyosarcomas.

Materials and methods

Isolation of genomic clones

A 21-kb genomic clone spanning exon 8 to the 3′-untranslated region of *Pax7* was isolated from a λ bacteriophage library of mouse strain SvJ-129 (Stratagene).

Production of gene-targeted mouse lines
Generation of the *Pax3:Fkhr* conditional allele is described in the accompanying paper (Keller et al. 2004). For the *Pax7–Cre* mouse line, a targeting vector was constructed that placed an *ires-Cre-FRT-Neo-FRT* cassette in the ClaI site within the 3′-untranslated region of the *Pax7* gene following the stop codon in exon 10. This targeting vector was electroporated into R1 embryonic stem cells that were then subjected to positive and negative selection. Three of 144 clones were identified as positive by screening with EcoRI genomic DNA digests with Southern hybridization using a 3′ external probe. Germ-line mice were generated as described in our accompanying paper (Keller et al. 2004). For genotyping by PCR, see Supplemental Material.

Pax7–Cre and Pax7–LacZ expression analysis
Whole-mount detection of the tissue-specific CRE expression for the *Pax7–Cre* mouse line was performed by crossing that line to *ROSA26* LacZ reporter mice (Sorriano 1999). Embryos were harvested at E10, E10.5, E12, or E12.5 and as described in our accompanying paper (Keller et al. 2004). Whole-mount LacZ expression in *Pax7–LacZ* E11.5 embryos was detected similarly (Mansouri et al. 1996).

Immunohistochemistry and fluorescence
Immunohistochemistry of sections was performed as described in our accompanying paper (Keller et al. 2004), and as detailed in Supplemental Material. For whole-mount *eYfp* fluorescence detection, E8.75 embryos placed in LabTek Chamber Slides (Nunc) and visualized by epifluorescence microscopy on a Zeiss Axiovert 200M microscope (Intelligent Imaging Innovations) using a YFP filter and Slidebook integration and deconvolution software (Intelligent Imaging Innovations).

RNA in situ hybridization
RNA in situ hybridization was performed as previously described (Lufkin 2003) using an 843-bp probe unique to native *Pax3* only (GenBank accession no. 6679210: nucleotides 1464–2214) that was derived from a reverse-transcriptase-amplified cDNA from wild-type E11 mouse embryo total RNA, which had been subcloned into the pCRII-TOPO plasmid (Invitrogen Life Technologies).

Acknowledgments

The monoclonal antibodies developed by Atsushi Kawakami and Miyuki Yamamoto were obtained from the Developmental Studies Hybridoma Bank (University of Iowa, Iowa City, IA). We appreciate a C-terminal-specific Pax3 antibody from Jonathan Epstein. We thank Mary Blandford, Kristin Deatherage, Jennifer Edwards, Misha S. Capecchi, Nichole Sanderson, Nathan Marsala, Fred Clayton, Lyn Pedone, and Daniel Fults for technical assistance and advice. This work was supported by a Scott Carter Foundation Fellowship to C.K. and by a K08 award from the National Cancer Institute (1K08 CA90438-01) to C.K.

References

Aubert, J., Stavridis, M.P., Tweedie, S., O'Reilly, M., Vierlinger, K., Li, M., Ghazal, P., Pratt, T., Mason, J.O., Roy, D., et al. 2003. Screening for mammalian neural genes via fluorescence-activated cell sorter purification of neural precursors from Sox1-gfp knock-in mice. *Proc. Natl. Acad. Sci.* **100 Suppl 1:** 11836–11841.

Auerbach, R. 1954. Analysis of the developmental defects of a lethal mutation in the house mouse. *J. Exper. Zool.* **127:** 305–329.

Borycki, A.G., Li, J., Jin, F., Emerson, C.P., and Epstein, J.A. 1999. Pax3 functions in cell survival and in pax7 regulation. *Development* **126:** 1665–1674.

Covault, J., Merlie, J.P., Goridis, C., and Sanes, J.R. 1986. Molecular forms of N-CAM and its RNA in developing and denervated skeletal muscle. *J. Cell Biol.* **102:** 731–739.

Davis, R.J. and Barr, F.G. 1997. Fusion genes resulting from alternative chromosomal translocations are overexpressed by gene-specific mechanisms in alveolar rhabdomyosarcoma. *Proc. Natl. Acad. Sci.* **94:** 8047–8051.

Ginsberg, J.P., Davis, R.J., Bennicelli, J.L., Nauta, L.E., and Barr, F.G. 1998. Up-regulation of MET but not neural cell adhesion molecule expression by the PAX3–FKHR fusion protein in alveolar rhabdomyosarcoma. *Cancer Res.* **58:** 3542–3546.

Goulding, M.D., Chalepakis, G., Deutsch, U., Erselius, J.R., and Gruss, P. 1991. Pax3, a novel murine DNA binding protein expressed during early neurogenesis. *EMBO J.* **10:** 1135–1147.

Greaves, M.F. and Wiemels, J. 2003. Origins of chromosome translocations in childhood leukaemia. *Nat. Rev. Cancer* **3:** 639–649.

Jostes, B., Walther, C., and Gruss, P. 1990. The murine paired box gene, Pax7, is expressed specifically during the development of the nervous and muscular system. *Mech. Dev.* **33:** 27–37.

Keller, C., Arenkiel, B.R., Coffin, C.M., El-Bardeesy, N., DePinho, R.A., and Capecchi, M.R. 2004. Alveolar rhabdomyosarcomas in conditional *Pax3:Fkhr* mice: Cooperativity of Ink4a/ARF and Trp53 loss of function. *Genes & Dev.* (this issue).

Lufkin, T. 2003. In situ hybridization of whole mount embryos with RNA probes. In *Manipulating the mouse embryo* (eds. M.G. Andras Nagy et al.), pp. 670–682. Cold Spring Harbor Laboratory Press, Cold Spring Harbor, NY.

Mansouri, A., Stoykova, A., Torres, M., and Gruss, P. 1996. Dysgenesis of cephalic neural crest derivatives in $Pax7^{-/-}$ mutant mice. *Development* **122:** 831–838.

Oustanina, S., Hause, G., and Braun, T. 2004. Pax7 directs postnatal renewal and propagation of myogenic satellite cells but not their specification. *EMBO J.* **23:** 3430–3439.

Pani, L., Horal, M., and Loeken, M.R. 2002. Rescue of neural tube defects in Pax-3-deficient embryos by p53 loss of function: Implications for Pax-3-dependent development and tumorigenesis. *Genes & Dev.* **16:** 676–680.

Ridgeway, A.G. and Skerjanc, I.A. 2001. Pax3 is essential for skeletal myogenesis and the expression of Six1 and Eya2. *J. Biol. Chem.* **276:** 19033–19039.

Schwenk, F., Baron, U., and Rajewsky, K. 1995. A Cre-transgenic mouse strain for the ubiquitous deletion of loxP-flanked gene segments including deletion in germ cells. *Nucleic Acids Res.* **23:** 5080–5081.

Sharp, R., Recio, J.A., Jhappan, C., Otsuka, T., Liu, S., Yu, Y., Liu, W., Anver, M., Navid, F., Helman, L.J., et al. 2002. Synergism between INK4a/ARF inactivation and aberrant HGF/SF signaling in rhabdomyosarcomagenesis. *Nat. Med.* **8:** 1276–1280.

Sorensen, P.H., Lynch, J.C., Qualman, S.J., Tirabosco, R., Lim, J.F., Maurer, H.M., Bridge, J.A., Crist, W.M., Triche, T.J., and Barr, F.G. 2002. PAX3–FKHR and PAX7–FKHR gene fusions are prognostic indicators in alveolar rhabdomyosarcoma: A report from the children's oncology group. *J. Clin. Oncol.* **20:** 2672–2679.

Sorriano, P. 1999. Generalized lacZ expression with the ROSA26 Cre reporter strain. *Nat. Genet.* **21:** 70–71.

Tomescu, O., Xia, S.J., Strezlecki, D., Bennicelli, J.L., Ginsberg, J., Pawel, B., and Barr, F.G. 2004. Inducible short-term and stable long-term cell culture systems reveal that the PAX3–FKHR fusion oncoprotein regulates CXCR4, PAX3, and PAX7 expression. *Lab. Invest.* **84:** 1060–1070.

Tremblay, P., Dietrich, S., Mericskay, M., Schubert, F.R., Li, Z., and Paulin, D. 1998. A crucial role for Pax3 in the development of the hypaxial musculature and the long-range migration of muscle precursors. *Dev. Biol. (Orlando)* **203:** 49–61.

Xia, S.J. and Barr, F.G. 2004. Analysis of the transforming and growth suppressive activities of the PAX3–FKHR oncoprotein. *Oncogene* 2004 Aug 2 [Epub ahead of print].